ACS OMEGA

http://pubs.acs.org/journal/acsodf

Article

Permeability Evolution of Shear Failing Chalk Cores under Thermochemical Influence

Emanuela I. Kallesten,* Pål Østebø Andersen, Merete V. Madland, Reidar I. Korsnes, Edvard Omdal, and Udo Zimmermann

Cite This: *ACS Omega* 2020, 5, 9185−9195

Read Online

ACCESS | Metrics & More | Article Recommendations

ABSTRACT: Development of petroleum reservoirs, including primary depletion of the pore pressure and repressurization during water injection naturally, leads to changes in effective stresses of the formations. These changes impose mechanical deformation of the rock mass with subsequent altering of its petrophysical properties. Besides mechanical compaction, chalk reservoirs on the Norwegian Continental Shelf also seem susceptible to mineralogical and textural changes as an effect of the injecting fluid's chemical composition and temperature. Understanding such chemical and thermal effects and how they interplay with the mechanical response to changes in effective stresses could contribute to improved prediction of permeability development during field life. This article presents results from mechanical testing of chalk cores of medium-porosity (32%) outcrop chalk (Niobrara Formation, Kansas) in triaxial cells. The experimental setup allows systematic combinations of fluctuating deviatoric stress, temperature (50 and 130 °C), and injecting fluid (calcite-equilibrated sodium chloride, calcite-equilibrated sodium sulfate, and reactive synthetic seawater) intended to replicate in situ processes, relevant to the North Sea chalk reservoirs. Deviatoric loading above yield resulted in a shear failure with a steeply dipping fracture of the core and a simultaneous increase in permeability. This occurred regardless of the brine composition. The second and third deviatoric loadings above yield did not have the same strong effect on permeability. During creep and unloading, the permeability changes were minor such that the end permeability remained higher than the initial values. However, sodium sulfate-injected cores retained most of the permeability gain after shear fracturing compared to sodium chloride and synthetic seawater series at both temperatures. Synthetic seawater-injected cores registered the most permeability loss compared to the other brines at 130 °C. The results indicate that repulsive forces generated by sulfate adsorption contribute to maintain the fracture permeability.

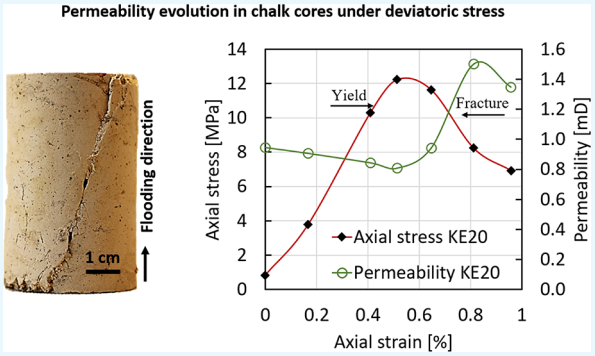

1. INTRODUCTION

Water-related improved oil recovery (IOR) techniques have a documented effect on hydrocarbon production in naturally fractured chalk reservoirs, and the success story of seawater injection at the Ekofisk field (North Sea, Norway) is closely linked to fracture permeability. With the matrix permeability evaluated in the range of 1−5 mD, the Ekofisk field chalk accommodates a natural fracture system that enhances the total reservoir permeability by a factor of 50.[1]

After several years of primary oil recovery by pore pressure depletion, the effective stress (overburden minus pore pressure) increased, causing the compaction mechanisms of the reservoir chalk to resume. This did not only lead to severe seafloor subsidence and challenges for the production facilities but also lead to significant changes in the physical and mechanical properties of the rock. Yet, despite years of compaction, loss of permeability was not detected.[2,3] Sulak[2] stated that, even though matrix permeability declined with matrix compaction, the effect was of no apparent consequence to the effective permeability. This seeming paradox indicated that fracture permeability, in another order of magnitude compared to the matrix permeability, dominates the effective permeability evolution. Additionally, Teufel[3] pointed out that the deviatoric nature of the reservoir stress state seems to govern the permeability of fractures such that steeply dipping fractures aligned with the maximum horizontal stress, as seen at Ekofisk, will suffer the least permeability loss. The study also underlined the different permeability behaviors under hydrostatic conditions, where permeability declines steadily with increasing hydrostatic stress.

Received: December 28, 2019
Accepted: April 1, 2020
Published: April 13, 2020

This behavior is clearly demonstrated[4−7] and does not capture permeability changes under deviatoric stresses, typical for reservoirs.

Stress anisotropy was also one of the reasons why field-wide implementation of seawater injection at the Ekofisk field in 1987 was remarkably successful. Teufel and Rhett[8] showed that decreasing effective mean stress by water injection while maintaining a large shear stress leads to increasing fracture density and fracture surface area and to significantly increased reservoir permeability.

Maintaining high fracture permeability, on the other hand, is not without challenges as production-related changes such as primary depletion of the pore pressure and repressurization during water injection continuously alter the effective stresses of the successions.[9,10] Such stress history affects the physical properties of porous rocks and their mechanical strength,[11,12] generating a complex porosity−permeability behavior in porous rocks. Studies of fracture permeability response to fluctuating effective stress[13−15] in porous rocks show less permeability changes with each stress cycle, and in any case, the loss of permeability seems irreversible. However, these studies only focus on stress-related permeability and do not incorporate other permeability-altering parameters, specific to carbonates. Ekofisk field observations of continued high compaction rates in certain areas even after repressurization and at constant pressure indicated the activity of other compaction mechanisms than only increasing effective stress and identified the chalk contact with nonequilibrium cold seawater as a likely cause.[16]

Field observations and laboratory studies remark that the temperature of the injecting fluid also contributes to continuous changes in the reservoir stress state; cold injecting fluid cools down the rock, causing it to contract and leading to a decrease in effective stress and increased permeability.[8,17] In a study of mechanical behavior of chalk cores exposed to temperature cycling, Voake et al.[18] observed more irreversible strain in chalk cores that experienced temperature fluctuations compared to cores tested at constant temperature.

Additionally, the fluid temperature plays an important role in how the fluid interacts with the reservoir rock. Chalk reservoirs found on the Norwegian Continental Shelf seem susceptible to mineralogical and textural changes, and their mechanical stability is dependent on the injected fluid's chemical composition and temperature.[7,19−26] Studies show that high temperature enhances the rock−fluid interactions and their effects are more obvious than at lower temperature. Particularly, ions such as Mg^{2+} and SO_4^{2-}, which are present in seawater, are responsible for the main chemical and mineralogical alterations in chalk (adsorption, calcite dissolution, and precipitation of new minerals). While seawater-like brines injected at increasing temperatures have a positive effect on the IOR potential,[27] they also reduce the mechanical strength of chalk, affect its elastic properties,[28] and lead to precipitation of permeability-inhibiting minerals such as anhydrite and gypsum.[23]

In the above review, most of the research has been conducted on whole cores to study the effect of systematically changing effective stress, temperature, and brine composition and see the resulting impact in terms of rock−fluid interactions, compaction, porosity, and permeability. Kallesten et al.[29] modeled chemical creep compaction in a fractured core subject to hydrostatic stresses but concluded that more experimental data were needed to characterize the fracture. A limited number of studies have considered fractured cores, deviatoric stress, or doing repeated stress cycles. Unique to the present study is that we generate fractured cores under deviatoric stress conditions and conduct repeated stress cycles while flooding inert or reactive brines at different temperatures, relevant to the chalk fields on the Norwegian Continental Shelf. The main aim is to see how different experimental conditions under stress cycles are able to affect the permeability of the system by investigating the interplay between varying parameters (stress state, temperature, and brine chemistry) and their combined effect on permeability evolution in chalk at such conditions. The test setup is designed to replicate the production-related dynamics of a chalk reservoir by considering shear-fractured outcrop chalk cores exposed to cyclic deviatoric stress states while systematically changing either the test temperature or the injected brine. In this way, different combinations of the experimental setup highlight the individual contribution of temperature, brine chemistry, and cyclic deviatoric stress on permeability evolution. The results will help answer the following:

- How do deviatoric stress cycles affect permeability?
- Is there any difference in permeability evolution when superimposing temperature or chemistry changes to the deviatoric stress cycles?
- Are these individual effects concurring or competing?

A better understanding of coexisting factors that affect reservoir permeability could bridge the gap toward an improved prediction of permeability development during field life.

2. EXPERIMENTAL PROCEDURES AND METHODS

This article presents results from mechanical testing of 12 chalk cores in triaxial cells. Such tests allow systematic changes of stress, temperature, and injecting fluid, intended to replicate in situ processes at reservoir conditions.

2.1. Sample Set. The sample set consists of 12 outcrop chalk cores (Niobrara Formation, Kansas/Utah) of medium porosity for a chalk (32%, ±1%). Experimental and theoretical studies demonstrate that mechanical strength of chalk is orientation-dependent and that chalk deformation behavior differs when main stress is applied parallel or perpendicular to bedding.[30,31] To ensure comparability between the tests, all cores are drilled from the same block collection and in the same direction. Further, the cores are cut to an average length of 75 mm and lathed to a diameter of 38.1 mm. The length−diameter ratio of approximately 2 should accommodate the steeply dipping shear fracture plane typical for deviatoric loading.[32]

2.2. Injecting Brines. The injecting brines define three test series: calcite-equilibrated sodium chloride (CE-NaCl), calcite-equilibrated sodium sulfate (CE-Na_2SO_4), and reactive synthetic seawater (SSW). By equilibrating the two former brines with calcite, no mineralogical interactions are expected, although surface reactions would be more likely. CE-NaCl is inert in all practical aspects and serves as a standard in comparison to CE-Na_2SO_4 and SSW brines. The concentrations of NaCl and Na_2SO_4 are designed to match the ionic strength of SSW (Table 1). The injection rate is 2 pore volumes (PVs)/day. After testing, the cores are flooded with 4 PVs distilled water (DW) to avoid salt precipitation.

2.3. Porosity and Permeability Calculation. For porosity calculation, the dry shaped cores were saturated with distilled water under vacuum conditions. The initial porosity (φ) is given by the ratio between pore volume (the difference in initial saturated and dry masses (M_{sat} and M_{dry}, respectively) divided by the density of distilled water (ρ_{dw})) and initial bulk volume ($V_{bulk,\ i}$)

https://dx.doi.org/10.1021/acsomega.9b04470
ACS Omega 2020, 5, 9185−9195

Table 1. Chemical Composition of Flooding Brines; Sodium Chloride (NaCl) and Sodium Sulfate (Na_2SO_4) Ionic Composition Here before Calcite Equilibration

flooding brine	NaCl	Na_2SO_4	SSW
ionic strength	0.657	0.657	0.657
Cl^- (mole L^{-1})	0.657	0.585	0.525
Na^+ (mole L^{-1})	0.657	0.633	0.450
SO_4^{2-} (mole L^{-1})		0.024	0.024
Ca^{2+} (mole L^{-1})			0.013
HCO_3^- (mole L^{-1})			0.002
Mg^{2+} (mole L^{-1})			0.045
K^+ (mole L^{-1})			0.010

$$\varphi = \frac{M_{\mathrm{sat},i} - M_{\mathrm{dry},i}}{\rho_{\mathrm{dw}} \times V_{\mathrm{bulk},i}} \quad (1)$$

The effective permeability (k) calculation is based on Darcy's law,[33] assuming a steady laminar fluid flow and symmetric axial and radial deformations

$$k = \frac{4\mu(L_i + \Delta L)Q}{\pi(D_i + \Delta D)^2 \Delta P} \quad (2)$$

where μ is the fluid viscosity as a function of salinity and temperature (cP; after El-Dessouky and Ettouny[34]), L_i is the initial length of the core (cm), ΔL is the change in core length (cm), Q is the flow rate (cm^3/s), D_i is the initial diameter of the core (cm), ΔD is the mean change in core diameter (cm), and ΔP is the pressure drop over the core during flooding (atm).

Uncertainties involved in the permeability calculation include fluid viscosity $\mu \pm 2\%$, change in core length $\Delta L \pm 0.7\%$, change in diameter $\Delta D \pm 1\%$, flooding rate $Q \pm 2\%$, and differential pressure $\Delta P \pm 0.075\%$. Permeability uncertainty Δk was estimated at $\pm 3\%$ by applying error estimation method shown in eq 3

$$\frac{\Delta k}{k} = \sqrt{\left[\frac{\Delta x}{x}\right]^2 + \left[\frac{\Delta y}{y}\right]^2 + \Delta\left[\frac{\Delta z}{z}\right]^2} \quad (3)$$

where x, ..., z are the measured values of the parameters with their respective Δx, ..., Δz uncertainty.[6]

A summary of the core properties before the mechanical testing (length, diameter, dry mass, saturated mass, porosity, permeability, and specific surface area) is listed in Table 2 and marked with index i (initial).

2.4. Triaxial Cell Tests. The triaxial cell is equipped with an outer heating jacket and a regulating system (Omron E5CN) with precise proportional integral derivative (PID) temperature control (±1.0 °C). The system includes two Quizix QX-2000HC pumps that control the axial and confining pressures independently and a fluid injection pump (Gilson 307HPLC) as well as a backpressure regulator that controls the pore pressure.

The cores are saturated with distilled water prior to cell mounting; they are isolated from the oil bath in the confining chamber by a heat shrinkage sleeve (fluorinated ethylene propylene, FEP; 0.5 mm in wall thickness). An extensometer surrounds the core at mid-length and measures the changes in diameter throughout the test (radial strain). Changes in the cores' length (axial strain) are monitored by an external axial linear variable displacement transducer (LVDT) placed on top of the cell piston.

Each series is performed at 50 °C, below the threshold for sulfate effects on chalk[35] and at 130 °C (reservoir temperature at Ekofisk) to trace the thermochemical effects on shear failing chalk cores injected with various brines. The low temperature tests require an initial heating to 130 °C to make sure that the shrinking sleeve is tight and uniform around the core, comparable to the tests at high temperature. During this stage, the injecting fluid is distilled water and brine injection only starting after the system had cooled down to 50 °C to avoid rock−brine interactions at high temperature.

Throughout the test, the confining pressure and pore pressure are constant at 1.2 and 0.7 MPa, respectively. In this way, the changes in effective stresses are a function of the increasing or decreasing axial stress. The cell piston is lowered carefully, and after core contact, it applies a pressure (0.5 MPa) that slightly overcomes the piston friction but causes negligible core deformation. The deviatoric tests start only when the triaxial cell has reached the right test temperature, the cores are brine-flooded with at least 2 PVs, the differential pressure is stable, and the system is in equilibrium (axial, radial strain rates close to 0).

2.5. Stress Cycles. The cores undergo the same stress sequence three times. The first step is axial loading at a constant injection rate (0.01 mL/min) above yield (defined by initiation of nonlinear stress−strain relationship) until shear failure (fracture formation) at which the value of axial stress drops. Immediately after, the axial pump is set to apply a constant

Table 2. List of Measurement Conditions and Core Properties before Testing[a]

flooding brine	T (°C)	core	L_i (mm)	D_i (mm)	$M_{\mathrm{dry},i}$ (g)	$M_{\mathrm{sat},i}$ (g)	φ_i (%)	k_i (mD)
CE-NaCl	50	KE4	70.3	38.12	134.6	162.7	32.6	1.24
	50	KE20	70.9	38.11	147.8	174.1	32.6	0.94
	130	KE44	76.5	38.10	159.9	188.0	32.2	0.64
	130	KE45	74.5	38.10	157.0	183.9	31.7	0.59
CE-Na_2SO_4	50	KE48	78.9	38.09	163.3	192.9	32.9	0.70
	50	KE75	75.9	38.14	158.3	186.4	32.4	0.62
	130	KE22	72.8	38.09	151.8	178.7	32.4	0.66
	130	KE55	75.9	38.10	157.3	185.5	32.6	0.61
SSW	50	KE47	75.4	38.10	155.9	184.1	32.9	0.81
	50	KE77	75.5	38.12	156.0	184.5	33.0	0.68
	130	KE51	77.1	38.10	161.7	189.9	32.1	0.58
	130	KE73	76.4	38.12	159.3	187.6	32.4	0.66

[a] T, temperature; L_i, initial length; D_i, initial diameter; $M_{\mathrm{dry},i}$, dry mass before testing; $M_{\mathrm{sat},i}$, saturated mass before testing; φ_i, initial porosity; k_i, initial permeability.

https://dx.doi.org/10.1021/acsomega.9b04470
ACS Omega 2020, 5, 9185−9195

pressure, slightly below the failure point, allowing the core to deform (creep) over 3 days. The axial pressure then returns to the starting point (0.5 MPa) at the same rate as loading. The second and third stress cycles, following the same procedure as the first, start after the system had reached equilibrium. In the second and third cycles, the creep phases are shorter (1 day).

3. RESULTS

Deviatoric loading above yield resulted without exception in a steeply dipping shear fracture along the core (Figure 1, left).

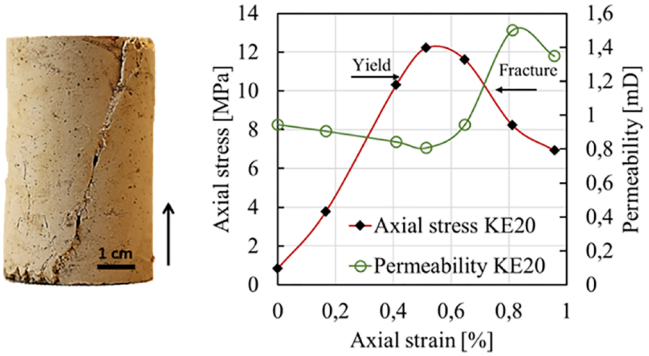

Figure 1. Right: High-angle shear fracture, typical for deviatoric loading at low confining pressure. The arrow indicates the flooding direction. Left: Typical example of axial stress−strain relationship (red curve) and permeability evolution (green curve) during first deviatoric loading above yield, here, data from the KE20 experiment (CE-NaCl series, 50 °C). Permeability generally decreases within the yield curve; the shear fracture event causes a concomitant drop in axial stress and an increase in permeability.

This is typical for compressive triaxial tests at low confining pressure, which allows the core to expand radially and facilitates well-organized shear failure between grains.[36] Figure 1 shows experiment KE20 (CE-NaCl series, 50 °C) to exemplify the typical permeability response (green curve) to first deviatoric loading above yield (red curve). Deviatoric loading within the yield curve (where the stress−strain relationship is linear) generally caused permeability decreases in all cores, in average, of 10% in the first cycle and 5% during second and third cycles compared to permeability values at the beginning of the respective cycles.

The shear fracture event, recognized by a drop in axial stress, initiated an abrupt increase in permeability, and generally, this occurred during the first loading. However, although all cores experienced the same deformation during the first loading, the mechanical strength of the cores and the degree of permeability rise differed. These differences should indicate the roles of injecting brine composition or temperature, the only two differing parameters in the test setup.

3.1. CE-NaCl Injection. Figure 2 shows permeability versus axial stress during deviatoric loading (left column) and permeability evolution in time during creep (right column) for the CE-NaCl test series. A clear distinction is seen between low temperature (blue curves) and high temperature (red curves) tests. As seen in Figure 2a, both cores tested at 50 °C (KE20 and KE4, blue lines) fractured at lower axial stress (11−12 MPa) than those tested at 130 °C (red lines, KE44 and KE45, 15−17 MPa). The shear fracture caused a drop in axial stress together with a clear rise in permeability (45% in average) and occurred mainly in the first loading. Test KE4 (50 °C), however, experienced a brief, unexpected pressure fluctuation in the beginning of the first loading at 5 MPa (Figure 2a), which might be related to an instrument error. This may have temporarily stabilized the core so that, at the end of the first deviatoric loading, the drop in axial stress from 11 to 9 MPa was an effect of microcracking, a precursor to fracturing.[37] A more pronounced shear fracture developed during the second loading cycle, leading to 1.75% axial deformation and 0.63% radial expansion, together with permeability rise by 36% (Figure 3b, blue triangles).

The mechanical strength decreased in all tests in the second loading (Figure 2b,c). The maximum axial stress was 3−4 MPa less compared to the first loading at 130 °C, while at 50 °C, the difference is approximately 5 MPa. Permeability increased in all tests after second loading but, unlike the first loading, by only less than 10% (excluding KE4).

Further, after the third loading, permeability decreased by 10% at 50 °C. Figure 2c (blue lines) shows that, after an initial decline during loading, the measured permeability remained constant. At 130 °C, on the other hand, it remained almost unchanged throughout the loading (Figure 2c, red lines).

The axial strain was the highest when the fracture occurred and it varied between 0.75 and 1.75% (Table 3), after which the cores experienced an average of 0.40% axial deformation at both temperatures. Radial strain does not correlate with the change in permeability so that more radial expansion does not necessarily lead to higher permeability.

Permeability seems unaffected by the degree of creep. Axial deformation during creep is a function of the applied axial stress, a value that was subjectively chosen for each core at each creep phase (Table 4). For example, in the KE44 test, the axial stress was 30% higher than KE45 at the same temperature, and it deformed three times more axially and six times more radially than KE45 during the first creep phase. Yet, permeability in both these tests is almost unchanged throughout the entire creep time (Figure 2d, red lines). The same trend is observed also in the creep phases 2 and 3, where the permeability does not register any significant changes. The two low temperature tests (KE4 and KE20), however, seem to decrease slightly during the first creep (Figure 2b, blue lines), but a direct comparison between the two tests is difficult because of the permeability fluctuations in KE4, which had not yet fractured properly at this point. During the second and third creep, on the other hand, the permeability only decreased somewhat in KE4 following the delayed clear shear fracture, but KE20 permeability stayed constant, similar to the high temperature tests (Figure 2e,f).

3.2. CE-Na_2SO_4 Fluid Injection. The results from the CE-Na_2SO_4 tests (Figure 3) show a similar permeability pattern as the CE-NaCl series. Permeability declined during the axial loading and increased with fracture formation in the first cycle (Figure 3a). Unlike the CE-NaCl tests, there is no clear maximum axial stress correlation between the high and low test temperatures. During the first loading cycle, the maximum axial stress was similar in three of the four tests, between 10 and 12 MPa, while KE22 withheld a maximum axial stress of 14 MPa. However, the high temperature tests registered the highest permeability increase when the shear fracture occurred, approximately double compared to the intact core permeability. At lower temperature, permeability increased with 50−80%. When comparing the first loading of the duplicate tests at each temperature, the magnitude of permeability rise correlates with the axial and radial strain: the higher the strain, the higher the permeability rise (Table 5).

https://dx.doi.org/10.1021/acsomega.9b04470
ACS Omega 2020, 5, 9185−9195

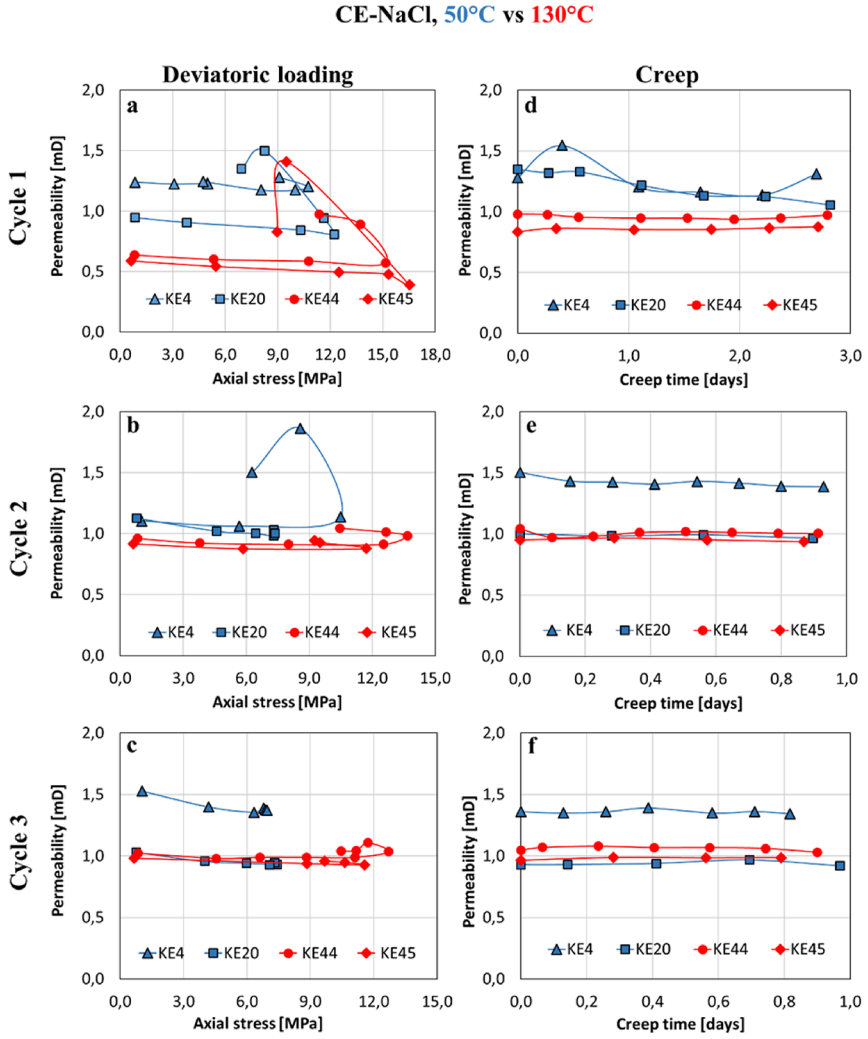

Figure 2. Permeability response to (a−c) axial stress and (d−f) creep in CE-NaCl experiments at 50 °C (blue lines) and 130 °C (red lines); the highest permeability increase is associated with core fracturing (a, and for KE4, b) after which no notable permeability change was observed. Creep under deviatoric conditions had a minimal effect on permeability evolution. The test temperature affected the mechanical strength during loading but did not play a decisive role in permeability during creep.

The mechanical strength decreased in all tests from the first cycle to the second and third cycles, regardless of test temperature (Figure 3b,c). Permeability increased in all experiments after the second loading cycle, this time by a factor of 2−4 more in the low temperature tests compared to the high temperature. This also corresponds to higher axial strain (0.62−0.98%) and radial strain (−0.2% in average) at low temperature compared to high temperature tests, which deformed in an average of 0.25% axially and below −0.1% radially at the same stage (Table 5).

The stress conditions in all three creep phases were similar (Table 6), and the cores sustained approximately 7 MPa constant axial stress and registered minor radial strain in all tests (between −0.02 and −0.06%). The axial strain varied somewhat with the temperature in the first creep phase so that, at low temperature, the axial strain was approximately double compared to the axial strain at 130 °C, but this had no clear effect on permeability.

The permeability generally declined after the first creep, mostly during the first creep day, after which it stabilized until the end of the creep phase (Figure 3d). Creep phases 2 and 3 (Figure 3e,f) induced minimal changes in permeability so that most of the permeability gain during the first loading cycle was retained throughout the test.

3.3. Synthetic Seawater Injection. The SSW-injected cores show similar permeability behavior as the CE-NaCl and CE-Na_2SO_4 series. As in the CE-Na_2SO_4 series, temperature did not play a distinguishing role in the maximum axial stress during the first loading cycle. Three of the tests fractured after a peak of approximately 12 MPa (Figure 4a), although performed at a different temperature. Core KE73 (130 °C, red diamonds) fractured after a maximum axial stress of 14 MPa. Although, generally, permeability increased after the first loading in all tests, there is no clear pattern in the rise magnitude (Table 7).

The strain−permeability correlation is seen here as well, where tests that showed higher permeability increase also experienced higher radial strain (Table 7). Core KE51 stands out with the highest permeability rise after the first loading (126%).

SSW flooding weakened the chalk cores similarly at both temperatures, showing an approximately 3−5 MPa decline in maximum axial stresses between the first loading and the subsequent loading phases. As in the CE-NaCl and CE-Na_2SO_4

https://dx.doi.org/10.1021/acsomega.9b04470
ACS Omega 2020, 5, 9185−9195

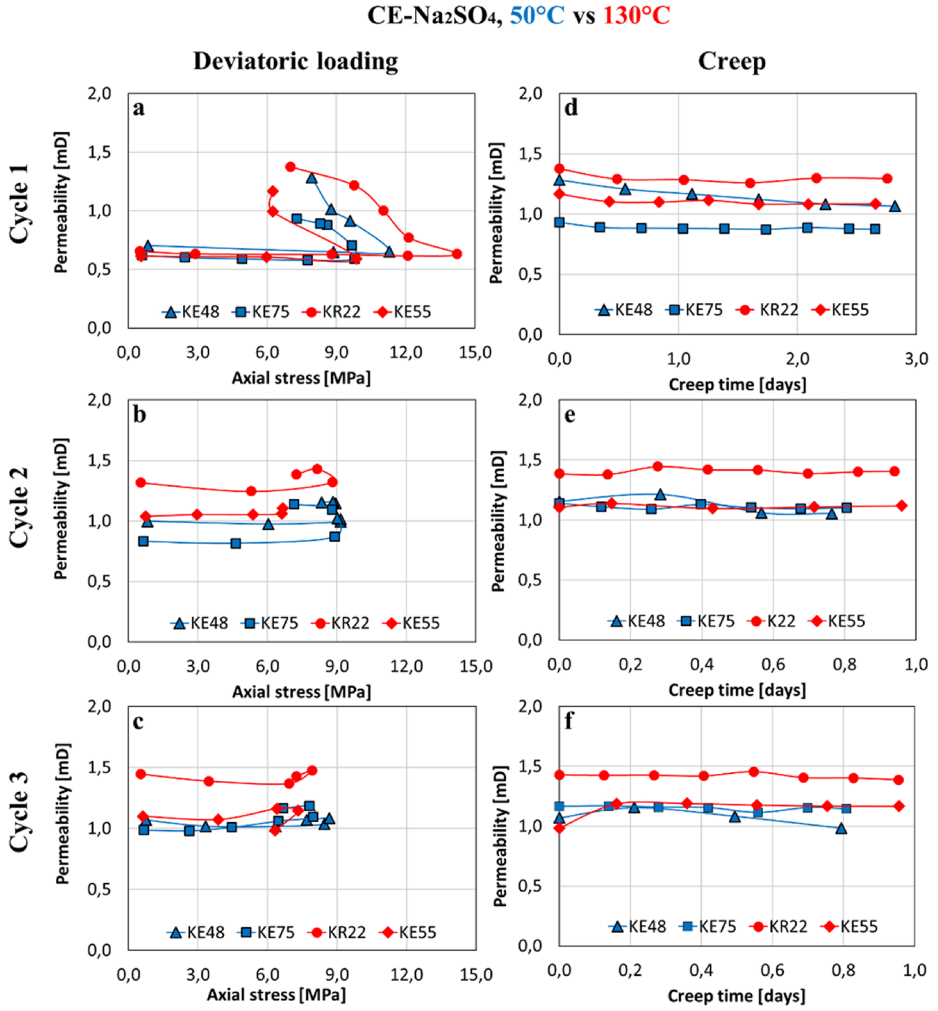

Figure 3. Permeability evolution in chalk cores flooded with CE-Na_2SO_4 brine at 50 °C (blue lines) and 130 °C (red lines) as a response to (a–c) deviatoric loading and (d–f) creep. Permeability rose clearly in the first loading cycle (a). After that, the permeability only registers minor changes regardless of temperature (b, c). Permeability remains almost unchanged during creep at both temperatures.

Table 3. Axial and Radial Strain (%) after Each Deviatoric Loading (CE-NaCl Series) and Permeability Change (%) Associated with Deviatoric Fracturing

			load 1			load 2		load 3	
flooding brine	T (°C)	core ID	axial strain (%)	radial strain (%)	permeability change (%)	axial strain (%)	radial strain (%)	axial strain (%)	radial strain (%)
CE-NaCl	50	KE4	0.88	−0.04	3	1.75	−0.63	0.48	−0.13
	50	KE20	0.96	−0.22	43	0.45	−0.67	0.28	−0.05
	130	KE44	0.75	−0.16	53	0.35	−0.09	0.38	−0.10
	130	KE45	1.04	−0.19	40	0.38	−0.08	0.44	−0.10

Table 4. Axial Stress (MPa) during Creep and Strain (%) after Each Creep Phase (CE-NaCl Series)

			creep 1			creep 2			creep 3		
flooding brine	T (°C)	core ID	axial stress (MPa)	axial strain (%)	radial strain (%)	axial stress (MPa)	axial strain (%)	radial strain (%)	axial stress (MPa)	axial strain (%)	radial strain (%)
CE-NaCl	50	KE4	6.9	0.14	−0.09	5.5	0.06	−0.01	5.5	0.03	0
	50	KE20	6.9	0.74	−0.68	6.8	0.21	−0.67	5.9	0.19	−0.05
	130	KE44	11.4	0.55	−0.2	10.4	0.14	−0.05	10.4	0.15	−0.05
	130	KE45	8.9	0.16	−0.03	9.2	0.07	−0.02	9.7	0.15	−0.05

series, permeability did not change significantly during deviatoric loadings 2 and 3.

Creep permeability trends were nearly parallel in all SSW experiments (Figure 4d–f), generally decreasing. End permeability was lowest in core KE51 (130 °C, Figure 4f, red bullets), which, throughout the test, lost more than half of the permeability gain after fracturing in loading 1. Core KE47 (50 °C) deformed at a high rate in all three creep cycles (Table 8),

https://dx.doi.org/10.1021/acsomega.9b04470
ACS Omega 2020, 5, 9185−9195

Table 5. Axial and Radial Strain (%) after Each Deviatoric Loading and Permeability Change (%) Associated with Shear Fracture during the First Loading

			load 1			load 2		load 3	
flooding brine	T (°C)	core	axial strain (%)	radial strain (%)	permeability change (%)	axial strain (%)	radial strain (%)	axial strain (%)	radial strain (%)
CE-Na_2SO_4	50	KE48	1.30	−0.25	+83	0.98	−0.23	0.40	−0.06
	50	KE75	1.02	−0.05	+50	0.62	−0.15	0.43	−0.12
	130	KE22	1.15	−0.39	+110	0.29	−0.07	0.28	−0.06
	130	KE55	0.97	−0.14	+90	0.22	−0.02	0.28	−0.05

Table 6. Axial Stress (MPa) during Creep and Strain (%) after Each Creep Phase (CE-Na_2SO_4 Series)

			creep 1			creep 2			creep 3		
flooding brine	T (°C)	core ID	axial stress (MPa)	axial strain (%)	radial strain (%)	axial stress (MPa)	axial strain (%)	radial strain (%)	axial stress (MPa)	axial strain (%)	radial strain (%)
CE-NA_2SO_4	50	KE48	7.7	0.33	−0.05	7.7	0.18	−0.03	7.7	0.15	−0.03
	50	KE75	7.2	0.59	−0.05	7.2	0.3	−0.06	6.7	0.15	−0.02
	130	KE22	7	0.16	−0.04	7.2	0.12	−0.04	7.2	0.12	−0.04
	130	KE55	6.2	0.27	−0.06	6.6	0.16	−0.04	6	0.19	−0.05

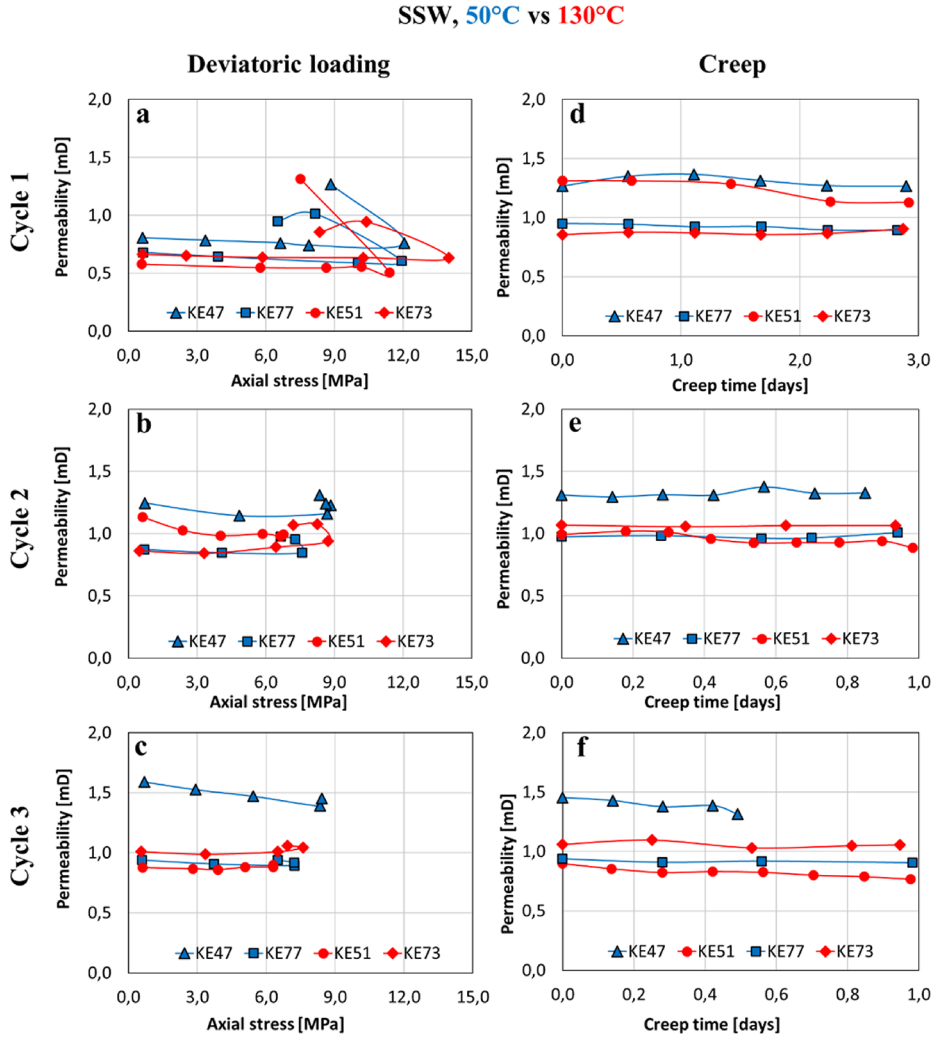

Figure 4. Permeability evolution in chalk cores flooded with SSW brine at 50 °C (blue lines) and 130 °C (red lines) as a response to (a−c) deviatoric loading and (d−f) creep. Permeability rose clearly in the first loading cycle as a result of shear fracturing (a). After that, the permeability registers minor changes regardless of temperature (b, c). Permeability remains almost unchanged during creep at both temperatures. Permeability of KE47 (blue triangles) declined more than all other tests in cycle 3 (c, f) as the core started to collapse.

https://dx.doi.org/10.1021/acsomega.9b04470
ACS Omega 2020, 5, 9185−9195

Table 7. Axial and Radial Strain (%) after Each Deviatoric Loading (SSW Series)

			load 1			load 2		load 3	
flooding brine	T (°C)	core ID	axial strain (%)	radial strain (%)	permeability change (%)	axial strain (%)	radial strain (%)	axial strain (%)	radial strain (%)
SSW	50	KE47	1.21	−0.16	+57	1.17	−0.31	0.41	−0.07
	50	KE77	0.77	−0.08	+40	0.39	−0.07	0.32	−0.05
	130	KE51	1.20	−0.24	+126	0.34	−0.06	0.20	−0.01
	130	KE73	0.67	−0.16	+29	0.49	−0.35	0.36	−0.11

Table 8. Axial Stress (MPa) during Creep and Strain (%) after Each Creep Phase (SSW Series)

			creep 1			creep 2			creep 3		
flooding brine	T (°C)	core ID	axial stress (MPa)	axial strain (%)	radial strain (%)	axial stress (MPa)	axial strain (%)	radial strain (%)	axial stress (MPa)	axial strain (%)	radial strain (%)
SSW	50	KE47	8.3	0.82	−0.23	8.2	1.16	−0.31	8.1		
	50	KE77	6.5	0.08	−0.01	6.6	0.08	−0.02	6.5	0.05	−0.01
	130	KE51	6.7	1.18	−0.36	6.8	0.31	−0.09	6.3	0.08	−0.02
	130	KE73	8.3	0.25	−0.07	7.2	0.11	−0.04	6.9	0.11	−0.04

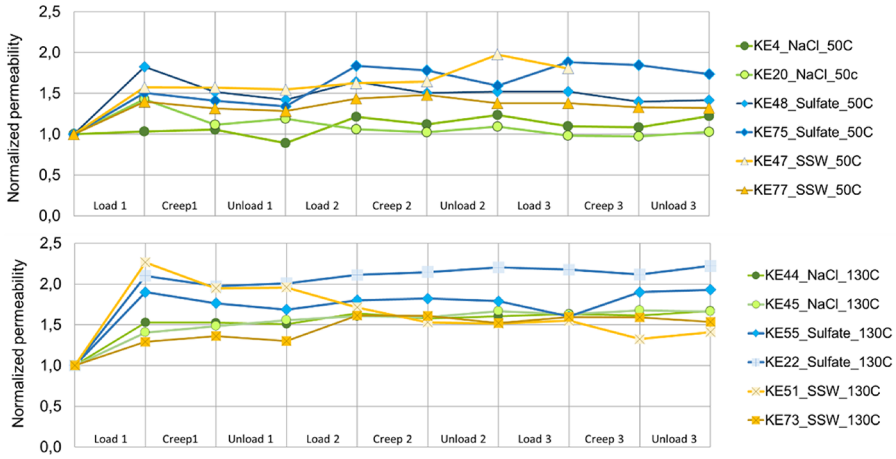

Figure 5. Overview of permeability evolution in all tested cores at 50 °C (top chart) and 130 °C (bottom chart). Permeability is normalized to the initial core permeability at the start of the first load; each line segment indicates the change in permeability during fluctuating stress states.

and the test was ultimately interrupted as the core collapsed. Yet, despite the accelerating creep conditions, the permeability decline rate is comparable to the other tests in this series.

4. DISCUSSION

The main drive in permeability change is the shear fracturing. Occurring mainly in the first deviatoric loading, the fracture serves as a "highway" for brine flow that induces a simultaneous permeability rise. The fracture dip angle is high and close to parallel to fluid flow due to the low confining pressure. The magnitude of permeability increase at this stage generally determines the cores' end permeability.

Figure 5 graphically displays the cumulative permeability evolution in all experiments, taking into account the unloading sequence as well. The first data point is the beginning of the first deviatoric cycle, and each line segment represents the permeability behavior during consecutive stress states. At both temperatures, end permeability of CE-Na_2SO_4-flooded cores is the highest. Megawati et al.[35] suggests that sodium sulfate brine injection at 130 °C does not cause new mineral precipitation such as anhydrite, but sulfate adsorption on chalk grains will change the chalk's surface charge and cause a disjoining force close to granular contacts. The disjoining force following sulfate adsorption may in fact explain why all CE-Na_2SO_4-flooded cores registered the highest permeability increase (Figure 5, blue lines).

On the other hand, SSW-flooded cores (yellow lines) gained least permeability at 130 °C, approximately half compared to CE-Na_2SO_4 series at the same temperature. That is most likely because SSW poses a different and more complex thermochemical scenario. According to previously mentioned studies,[23,30] SSW injection at 130 °C leads to both sulfate adsorption and mineralogical changes. Ca^{2+} substitution with Mg^{2+} and anhydrite ($CaSO_4$) precipitation contribute further to chalk weakening and alter fracture permeability. Particularly, anhydrite precipitation is a common permeability inhibitor, and Figure 5 shows that end permeability of both SSW-injected cores at 130 °C (yellow lines) lies below the other two series (CE-Na_2SO_4, blue lines, and CE-NaCl, green lines).

Another notable aspect from Figure 5 is that the degree of permeability rise related to fracturing (load 1) correlates with test temperature: overall, permeability increased 70%, in average, at the beginning of the tests at high temperature and only 40% average at low temperature. There was also higher variation in permeability rise among high temperature tests, compared to low temperature tests, where four out of six tests had an almost identical permeability increase. Additionally, end

https://dx.doi.org/10.1021/acsomega.9b04470
ACS Omega 2020, 5, 9185−9195

permeability at 130 °C increased, in average, by a factor of 1.7, while at 50 °C, the average increasing factor was 1.3.

Both stress and thermochemical test conditions impact the cores' mechanical strength to different degrees, generally decreasing throughout the test. Repetitive deviatoric loadings following the fracture formation do not seem to affect permeability as much as the shear fracturing event. This is in agreement with other studies[13,14] that, although performed under different thermochemical conditions than the present study, report that a second deviatoric stress cycle had a less effect on permeability evolution compared to the first cycle. The cycles naturally weaken the cores, with each loading−unloading adding more fatigue and deformation to the rock and altering its elastic properties.[11] The effect of temperature and injecting brine on the cores' mechanical strength is shown in Table 9.

Table 9. Maximum Axial Stress (MPa) during Deviatoric Loading under Different Thermochemical Conditions

			load 1	load 2	load 3
T (°C)	flooding brine	core ID	max. axial stress (MPa)	max. axial stress (MPa)	max. axial stress (MPa)
50 °C	CE-NaCl	KE4	11	10	7.0
	CE-NaCl	KE20	12	7.5	7.5
	CE-NA_2SO_4	KE48	12	9.1	8.6
	CE-NA_2SO_4	KE75	10	9.3	7.9
	SSW	KE47	13	8.9	8.4
	SSW	KE77	12	7.5	7.3
130 °C	CE-NaCl	KE44	15	14	13
	CE-NaCl	KE45	17	12	12
	CE-NA_2SO_4	KE22	14	8.8	8.6
	CE-NA_2SO_4	KE55	10	7.0	7.4
	SSW	KE51	11	6.6	6.7
	SSW	KE73	14	8.8	7.6

The CE-Na_2SO_4-injected cores at 50 °C registered the least mechanical strength decline (2−3 MPa) compared to the SSW (5 MPa) and CE-NaCl (4 MPa) series. At 130 °C, however, the CE-NaCl-injected cores retain most of their initial strength, while CE-Na_2SO_4 and, particularly, SSW series become weaker. This observation is in agreement with the previous studies[23,30] on SSW influence on the mechanical stability of chalk. Additionally, higher temperature intensifies the rock interactions with the injection brine.[7,19,23,24,30,35]

Creep conditions did not seem to override the permeability gain during fracturing. This is in agreement with other studies[3,6] that observed a low permeability decline in deviatoric conditions.

Table 10 summarizes the key changes recorded during each experiment. The net axial and radial strains are calculated as the percentage axial compaction and radial expansion, respectively, at the end of the test relative to the initial length and diameter respectively shown in Table 2.

In CE-NaCl and CE-Na_2SO_4 test series, the low temperature tests suffered more axial compaction than the high temperature tests. This correlates well with the end permeability: permeability increased only slightly in CE-NaCl-flooded cores at 50 °C (0 and 21%) but more clearly at higher temperature (66%). A similar pattern appears in CE-Na_2SO_4 tests. Low temperature cores experienced more compaction (2.5 and 2.8%) and less permeability increase (41 and 73%) than the cores flooded with CE-Na_2SO_4 at 130 °C (1.6% axial strain and a permeability increase by 95 and 122%). This indicates that, when flooding equilibrium brines that do not alter chalk mineralogy, brine temperature can play a significant role in mechanical compaction (strain), a key permeability-controlling factor.

This correlation is not clear in SSW series. Experiment KE47 failed before all stress sequences were complete so that the high compaction (4.3%) and high end permeability (+80%) are irrelevant in this argument. At 130 °C, KE51 deforms more axially (2.9%) than the second test at the same temperature (KE73, 1.3%) and end permeability is consequently lower with higher compaction, as in the previous two series.

There is little variation in net radial strain among the tests (between −0.2 and −0.8%, excluding KE47), indicating that flooding brine and temperature do not decisively affect fracture aperture, and any radial strain is rather stress-induced. Ultimately, there is no immediate correlation between the net radial strain and end permeability.

5. CONCLUSIONS

This study focuses on permeability evolution in fractured chalk cores exposed to cyclic deviatoric stress and thermochemical influence relevant to reservoir conditions. The test setup included three series, each with specific injecting brine: two calcite-equilibrated brines (CE-NaCl and Na_2SO_4) and one

Table 10. Summary of the Cores' Measured Axial and Radial Strain (%) and Permeability Changes

flooding brine	T (°C)	core ID	net axial strain (%)	net radial strain (%)	k_i (mD)	k_{end} (mD)	net permeability change (%)
CE-NaCl	50	KE4	3.0	−0.8	1.24	1.51	+22
	50	KE20	2.3	−0.7	0.94	0.97	+2.8
	130	KE44	1.7	−0.6	0.64	1.06	+67
	130	KE45	1.7	−0.5	0.59	0.98	+66
CE-Na_2SO_4	50	KE48	2.8	−0.6	0.70	1.00	+41
	50	KE75	2.5	−0.4	0.62	1.07	+73
	130	KE22	1.6	−0.6	0.66	1.46	+122
	130	KE55	1.6	−0.3	0.61	1.19	+95
SSW	50	KE47	4.3[a]	−1.0[a]	0.81	1.45[a]	+80[a]
	50	KE77	1.2	−0.2	0.68	0.90	+32
	130	KE51	2.9	−0.7	0.58	0.82	+41
	130	KE73	1.3	−0.5	0.66	1.02	+54

[a]Calculated values at the end of the third deviatoric loading prior to core collapse.

https://dx.doi.org/10.1021/acsomega.9b04470
ACS Omega 2020, 5, 9185−9195

nonequilibrium brine (SSW). Each test series was performed at 50 and 130 °C. Such flooding experiments highlight the interplay between the parameters. The results showed that stress-induced fracturing is the main permeability drive as permeability changed decisively only as a response to fracturing of the core. The deviatoric stress state together with low confining pressure induced shear fracturing at a steep angle (over 70°), close to the flooding direction. Subsequent deviatoric loadings had a little effect on permeability in all tests, regardless of injecting brine and test temperature. During creep, permeability generally declined slightly or remained unchanged. Our results indicate that, once chalk has fractured, the effective permeability is insensitive to compaction cycles and reactive flow, both at high and low temperatures.

The CE-Na_2SO_4 test series stand out with the highest final permeability at both temperatures. This is likely a result of sulfate adsorption on the chalk grain surface creating enough disjoining force at granular contact to preserve permeability. Additionally, calcite equilibration of the brine prevented calcium displacement and, consequently, anhydrite precipitation.

If flooding CE-Na_2SO_4 through fractured chalk seems to sustain the permeability gain related to shear fracturing, then flooding reactive brine such as SSW at a high temperature has a competing effect on permeability evolution. SSW test series registered most permeability loss at 130 °C, most likely due to chemical alteration, possibly precipitation of anhydrite.

However, all cores had a positive net permeability change. Despite fracturing and exposure to different stress states, temperatures, and brine conditions, core permeability at the end of the test seems to remain within the same order of magnitude as the original value, ranging between the initial value and double of the initial value. This indicates strong insensitivity to changes in reservoir conditions.

The results are repeatable, confirming permeability behavior for this experiment setup. Future studies should investigate the effects of longer-term stress cycles or several stress cycles at actual reservoir stress conditions on permeability evolution in fractured chalk cores. Additional analyses such as scanning electron microscopy can then verify the chemical alteration caused by reactive fluid flow in chalk, as suggested by Minde et al.,[38] and determine mineral alteration along the fracture or in the matrix. Although challenging to obtain, similar flooding experiments on actual reservoir chalk from the North Sea would provide important data for validating outcrop chalk test results and refining permeability models for the North Sea reservoir chalk. Especially, the importance of the adsorption mechanism to maintain fracture permeability in the field should be investigated further.

AUTHOR INFORMATION

Corresponding Author

Emanuela I. Kallesten − *University of Stavanger, 4021 Stavanger, Norway; The National IOR Centre of Norway, 4021 Stavanger, Norway;* orcid.org/0000-0002-3534-4386; Email: emanuela.i.kallesten@uis.no

Authors

Pål Østebø Andersen − *University of Stavanger, 4021 Stavanger, Norway; The National IOR Centre of Norway, 4021 Stavanger, Norway;* orcid.org/0000-0002-8552-094X

Merete V. Madland − *University of Stavanger, 4021 Stavanger, Norway; The National IOR Centre of Norway, 4021 Stavanger, Norway*

Reidar I. Korsnes − *University of Stavanger, 4021 Stavanger, Norway; The National IOR Centre of Norway, 4021 Stavanger, Norway*

Edvard Omdal − *ConocoPhillips, 4056 Tananger, Norway*

Udo Zimmermann − *University of Stavanger, 4021 Stavanger, Norway; The National IOR Centre of Norway, 4021 Stavanger, Norway*

Complete contact information is available at: https://pubs.acs.org/10.1021/acsomega.9b04470

Notes

The authors declare no competing financial interest.

ACKNOWLEDGMENTS

The authors acknowledge the Research Council of Norway and the industry partners, ConocoPhillips Skandinavia AS, Aker BP ASA, Vår Energi AS, Equinor ASA, Neptune Energy Norge AS, Lundin Norway AS, Halliburton AS, Schlumberger Norge AS, and Wintershall DEA, of The National IOR Centre of Norway for the support.

REFERENCES

(1) Sulak, R. M.; Danielsen, J. Reservoir Aspects of Ekofisk Subsidence. *J. Pet. Technol.* **1989**, *41*, 709−716.

(2) Sulak, R. M. Ekofisk field: the first 20 years. *J. Pet. Technol.* **1991**, *43*, 1−265.

(3) Teufel, L. W. Permeability of naturally fractured reservoirs. In *AAPG 1991 annual convention with DPA/EMD divisions and SEPM, an associated society;* AAPG: 1991, *75* (3), 680.

(4) Suri, P.; Azeemuddin, M.; Zaman, M.; Kukreti, A. R.; Roegiers, J. C. Stress-dependent permeability measurement using the oscillating pulse technique. *J. Pet. Sci. Eng.* **1997**, *17*, 247−264.

(5) Yale, D. P.; Crawford, B. Plasticity and permeability in carbonates: dependence on stress path and porosity. In *SPE/ISRM Rock Mechanics in Petroleum Engineering.* Society of Petroleum Engineers, 1998.

(6) Korsnes, R. I.; Risnes, R.; Faldaas, I.; Norland, T. End effects on stress dependent permeability measurements. *Tectonophysics* **2006**, *426*, 239−251.

(7) Minde, M. W.; Wang, W.; Madland, M. V.; Zimmermann, U.; Korsnes, R. I.; Bertolino, S. R. A.; Andersen, P. Ø. Temperature effects on rock engineering properties and rock-fluid chemistry in opal-CT-bearing chalk. *J. Pet. Sci. Eng.* **2018**, *169*, 454−470.

(8) Teufel, L. W.; Rhett, D. W. Failure of Chalk During Waterflooding of the Ekofisk Field. In *SPE Annual Technical Conference and Exhibition.* Society of Petroleum Engineers, 1992.

(9) Smart, B. G. D.; Somerville, J. M.; Edlman, K.; Jones, C. Stress sensitivity of fractured reservoirs. *J. Pet. Sci. Eng.* **2001**, *29*, 29−37.

(10) Moosavi, S. A.; Goshtasbi, K.; Kazemzadeh, E.; Bakhtiari, H. A.; Esfahani, M. R.; Vali, J. Relationship between porosity and permeability with stress using pore volume compressibility characteristic of reservoir rocks. *Arabian J. Geosci.* **2014**, *7*, 231−239.

(11) Ray, S. K.; Sarkar, M.; Singh, T. N. Effect of cyclic loading and strain rate on the mechanical behaviour of sandstone. *Int. J. Rock Mech. Min. Sci.* **1999**, *36*, 543−549.

(12) Bernabé, Y.; Mok, U.; Evans, B. Permeability-porosity relationships in rocks subjected to various evolution processes. *Pure Appl. Geophys.* **2003**, *160*, 937−960.

(13) Milsch, H.; Hofmann, H.; Blöcher, G. An experimental and numerical evaluation of continuous fracture permeability measurements during effective pressure cycles. *Int. J. Rock Mech. Min. Sci.* **2016**, *100*, 109−115.

(14) Kluge, C.; Blöcher, G.; Milsch, H.; Hofmann, H.; Nicolas, A.; Li, Z.; Fortin, J. Sustainability of fractured rock permeability under varying pressure. In *Poromechanics VI*; American Society of Civil Engineers: 2017, 1192−1199.

https://dx.doi.org/10.1021/acsomega.9b04470
ACS Omega 2020, 5, 9185−9195

(15) Hu, C.; Agostini, F.; Skoczylas, F.; Egermann, P. Effects of gas pressure on failure and deviatoric stress on permeability of reservoir rocks: initial studies on a Vosges sandstone. *Eur. J. Environ. Civ. Eng.* **2018**, *22*, 1004−1022.
(16) Hermansen, H.; Landa, G. H.; Sylte, J. E.; Thomas, L. K. Experiences after 10 years of waterflooding the Ekofisk Field, Norway. *J. Pet. Sci. Eng.* **2000**, *26*, 11−18.
(17) Uribe-Patiño, J. A.; Alzate-Espinosa, G. A.; Arbeláez-Londoño, A. Geomechanical aspects of reservoir thermal alteration: A literature review. *J. Pet. Sci. Eng.* **2017**, *152*, 250−266.
(18) Voake, T.; Nermoen, A.; Korsnes, R. I.; Fabricius, I. L. Temperature cycling and its effect on mechanical behaviours of high-porosity chalks. *J. Rock Mech. Geotech. Eng.* **2019**, *11*, 749−759.
(19) Austad, T.; Strand, S.; Høgnesen, E. J.; Zhang, P. Seawater as IOR fluid in fractured chalk. In *SPE international symposium on oilfield chemistry;* Society of Petroleum Engineers: 2005.
(20) Heggheim, T.; Madland, M. V.; Risnes, R.; Austad, T. A chemical induced enhanced weakening of chalk by seawater. *J. Pet. Sci. Eng.* **2005**, *46*, 171−184.
(21) Austad, T.; Strand, S.; Madland, M. V.; Puntervold, T.; Korsnes, R. I. Seawater in Chalk: An EOR and Compaction Fluid. In *International Petroleum Technology*; International Petroleum Technology Conference: 2008, *11* (04), 648−654, DOI: 10.2118/118431-PA.
(22) Korsnes, R. I.; Wersland, E.; Austad, T.; Madland, M. V. Anisotropy in chalk studied by rock mechanics. *J. Pet. Sci. Eng.* **2008**, *62*, 28−35.
(23) Madland, M. V.; Hiorth, A.; Omdal, E.; Megawati, M.; Hildebrand-Habel, T.; Korsnes, R. I.; Evje, S.; Cathles, L. M. Chemical Alterations Induced by Rock−Fluid Interactions When Injecting Brines in High Porosity Chalks. *Transp. Porous Media* **2011**, *87*, 679−702.
(24) Megawati, M.; Madland, M. V.; Hiorth, A. Mechanical and physical behavior of high-porosity chalks exposed to chemical perturbation. *J. Pet. Sci. Eng.* **2015**, *133*, 313−327.
(25) Bergsaker, A. S.; Røyne, A.; Ougier-Simonin, A.; Aubry, J.; Renard, F. The effect of fluid composition, salinity, and acidity on subcritical crack growth in calcite crystals. *J. Geophys. Res.: Solid Earth* **2016**, *121*, 1631−1651.
(26) Polat, C.; Parlaktuna, M. A study on the effect of the chemical composition of brine to improve oil recovery from carbonates. *Energy Sources, Part A* **2017**, *39*, 2151−2156.
(27) Zhang, P.; Tweheyo, M. T.; Austad, T. Wettability alteration and improved oil recovery by spontaneous imbibition of seawater into chalk: Impact of the potential determining ions Ca^{2+}, Mg^{2+}, and SO_4^{2-}. *Colloids Surf., A* **2007**, *301*, 199−208.
(28) Nermoen, A.; Korsnes, R. I.; Storm, E. V.; Stødle, T.; Madland, M. V.; Fabricius, I. L. Incorporating electrostatic effects into the effective stress relation—Insights from chalk experiments. *Geophysics* **2018**, *83*, MR123−MR135.
(29) Kallesten, E.; Østebø Andersen, P. Ø.; Berawala, D. S.; Korsnes, R. I.; Vadla Madland, M.; Omdal, E.; Zimmermann, U. Modelling of Permeability and Strain Evolution in Chemical Creep Compaction Experiments with Fractured and Unfractured Chalk Cores Conducted at Reservoir Conditions. *SPE J.* **2020** SPE-197371-PA (in press; available online April 2020) DOI: 10.2118/197371-PA.
(30) Korsnes, R. I.; Madland, M. V.; Austad, T.; Haver, S.; Røsland, G. The effects of temperature on the water weakening of chalk by seawater. *J. Pet. Sci. Eng.* **2008**, *60*, 183−193.
(31) Daigle, H.; Rasromani, E.; Gray, K. E. Near-wellbore permeability alteration in depleted, anisotropic reservoirs. *J. Pet. Sci. Eng.* **2017**, *157*, 302−311.
(32) Fjær, E.; Holt, R. M.; Horsrud, P.; Raaen, A. M.; Risnes, R. *Mechanical properties and stress data from laboratory analysis. In Petroleum Related Rock Mechanics*, 2nd Ed., Vol. *53*; Elsevier: 2008; pp 251−287.
(33) Darcy, H. P. G. *Les Fontaines publiques de la ville de Dijon. Exposition et application des principes à suivre et des formules à employer dans les questions de distribution d'eau, etc.*; V. Dalamont: 1856.
(34) El-Dessouky, H. T.; Ettouney, H. M. Thermodynamic Properties. In *Fundamentals of salt water desalination*, 1st ed.; Elsevier, 2002; pp 525−564.
(35) Megawati, M.; Hiorth, A.; Madland, M. V. The impact of surface charge on the mechanical behavior of high-porosity chalk. *Rock Mech. Rock Eng.* **2013**, *46*, 1073−1090.
(36) Risnes, R. Deformation and yield in high porosity outcrop chalk. *Phys. Chem. Earth A: Solid Earth Geod.* **2001**, *26*, 53−57.
(37) Dautriat, J.; Gland, N.; Dimanov, A.; Raphanel, J. Hydromechanical behavior of heterogeneous carbonate rock under proportional triaxial loadings. *J. Geophys. Res.: Solid Earth* **2011**, *116*, B01205.
(38) Minde, M. W.; Zimmermann, U.; Madland, M. V.; Korsnes, R. I.; Schulz, B.; Audinot, J. N. Fluid−flow during EOR experiments in chalk: insights using SEM−MLA, EMPA and Nanosims Applications. In *International Symposium of the Society of Core Analysts*; The Society of Core Analysts: 2016, 21−26.

https://dx.doi.org/10.1021/acsomega.9b04470
ACS Omega 2020, 5, 9185−9195